# Nonequilibrium Adhesion Patterns at Lipid Bilayer Junctions

**Raghuveer Parthasarathy, Bryan L. Jackson, Thomas J. Lowery, Amy P. Wong, and Jay T. Groves\***

*Department of Chemistry, University of California, Berkeley, California 94720*

*Received: June 2, 2003*

With lipid bilayer−bilayer junctions in mind as model systems for the study of cell−cell junctions, we have examined adhesion between simple lipid membranes using fluorescence resonance energy transfer (FRET) and fluorescence interference contrast microscopy (FLIC) to map the interfacial topography. The contact can take the form of uniform adhesion, with an intermembrane separation of nanometers, or nonuniform adhesion, in which blisters hundreds of nanometers in height coexist with tight adhesion zones. We find that blisters can result as a consequence of rapid interbilayer contact induced by osmotic shock. We develop a model for the formation and stabilization of the blisters, confirming that these phenomena are governed mainly by hydrodynamic flow in the intermembrane space.

## 1. Introduction

A variety of fascinating adhesion, recognition, and signaling phenomena occur at cell−cell contacts.[1,2] In the past decade particularly it has been realized that many of these cell−cell interactions are accompanied by spatial and temporal pattern formation on the part of the lipids and proteins at the cell surfaces.[2−4] In at least one notable case, the "immunological synapse", there is evidence that physical mechanisms related to membrane bending mechanics and phase separation of proteins drive these patterns.[5−7] To deconvolve the various forces behind cell-surface reorganization, we turn to reconstituted lipid bilayers, proposing bilayer−bilayer junctions as an experimental model system for studying cell−cell junction biophysics. A starting point for such a program is an understanding of adhesion and contact in the simplest protein-free bilayer−bilayer junctions.

Reconstituted lipid bilayers are studied extensively as model systems for exploring the physical and chemical properties of cell membranes, of which they form the dominant structural component.[8] Artificial bilayers can include lipids of desired chemical structure and electric charge, as well as fluorescent lipid probes. Furthermore, an array of techniques involving resonance energy transfer and optical interference has been developed in the past few years for imaging junctions *between* lipid bilayers, providing nanometer-scale topographic information. These methods include Förster (or fluorescence) resonance energy transfer (FRET), fluorescence interference contrast microscopy (FLIC), and reflection interference contrast microscopy (RICM). In FRET, overlap between the absorption spectrum of one fluorophore of the FRET pair, located on one membrane, and the emission spectrum of the other, located on the second membrane, leads to nonradiative energy transfer between the two and a quenching of the latter's fluorescence.[9−11] The length scale for FRET is the Förster radius of the fluorophore, typically a few nanometers; FRET can provide quantitative and precise topographic information in the angstrom to nanometer range.[11] In FLIC, interference of the fluorophore's excitation and emission light with their reflections from a nearby surface create interference fringes that map topography.[10,12] In RICM, interference between light reflected at the membrane and light reflected at the substrate interface again maps topography onto intensity.[13]

One of the central questions concerning the bilayer−bilayer junctions is this: what controls the spatial uniformity (or nonuniformity) of adhesion? Nonuniform adhesion, in the form of "blisters" in the junction, has been observed recently by Nardi et al.[14] using RICM. The formation of blisters was attributed to phase separation of the charged lipid components.

We find, in contrast, that nonuniform adhesion can also occur even in the absence of charged lipids; phase separation is not a necessary condition. Rather, rapid bilayer−bilayer contact induced, for example, by osmotic shock generates instabilities in the intermembrane spacing that lead to the observed blisters. These nonequilibrium structures are stabilized by impedance to hydrodynamic flow, for which we develop a quantitative model.

Experimentally, we used FRET and FLIC imaging to examine junctions between pairs of reconstituted lipid bilayers, composed of lipids and fluorescent lipid probes. The "lower" bilayer is a supported membrane,[8] formed by rupture of small unilamellar vesicles (SUVs) on a $SiO_2$ substrate (either a glass coverslip or, for FLIC measurements, a thermal oxide layer on a Si wafer). A 10−20 Å native water layer separates the lipid bilayer from the solid substrate,[15,16] enabling fluidity of the membrane lipids, as verified by testing fluorescence recovery after photobleaching. The "upper" lipid bilayer is formed by rupture of a giant unilamellar vesicle (GUV), either spontaneously as it descends onto the lower bilayer, or in response to an osmotic shock.

## 2. Materials and Methods

All lipids used were purchased from Avanti Polar Lipids (Alabaster, Alabama): dimyristoylphosphatidylcholine (DMPC), 1,2-dioleoyl-*sn*-glycero-3-phosphocholine (DOPC), dioleoyl-dimethylammonium propane (DODAP), L-α-phosphatidylcholine obtained from chicken egg (Egg-PC), and L-α-phosphatidylinositol obtained from soy plants (plant-PI).

The fluorescently labeled lipid probes 1-palmitoyl-2-[12-[(7-nitro-2-1,3-benzoxadiazol-4-yl)amino]dodecanoyl]-*sn*-glycero-3-[phospho-rac-(1-glycerol)] (NBD-PG) and 1-palmitoyl-2-[12-[(7-nitro-2-1,3-benzoxadiazol-4-yl)amino]dodecanoyl]-*sn*-

glycero-3-phosphocholine (NBD-PC) were also purchased from Avanti Polar lipids, while 2-[4,4-difluoro-5-(4-phenyl-1,3-butadienyl)-4-bora-3a,4a-diaza-s-indacene-3-pentanoyl]-1-hexadecanoyl-*sn*-glycero-3-phosphocholine ($\beta$-BODIPY 581/591 $C_5$-HPC), 2-(4,4-difluoro-5,7-dimethyl-4-bora-3a,4a-diaza-s-indacene-3-pentanoyl)-1-hexadecanoyl-*sn*-glycero-3-phosphocholine ($\beta$-BODIPY FLC$_5$–HPC), and N-(Texas red sulfonyl)-1,2-dihexadecanoyl-*sn*-glycero-3-phosphoethanolamine, triethylammonium salt (Texas red DHPE) were purchased from Molecular Probes (Eugene, Oregon).

Texas red and NBD are a FRET pair, as are $\beta$-BODIPY 581/591 $C_5$-HPC and $\beta$-BODIPY FLC$_5$-HPC; in each case, the former is the acceptor and the latter is the donor of the energy transfer.

The compositions (mole fraction) of the lipid bilayers shown in the figures are as follows: For Figure 1 and Figure 2a–f the supported bilayer composition is 93% DMPC, 2% NBD-PG, and 5% DODAP, and the composition of the upper bilayer patches is 88% DMPC, 5% Plant PI, 1% Texas red DHPE, and 6% DODAP; for Figure 2g,h the supported bilayer composition is 95% DMPC, 3% DODAP, and 2% NBD-PG, and the composition of the upper bilayer patches is 65% DMPC, 32% DOPC, 0.5% Texas red DHPE, and 2.5% DODAP; for Figure 2i,j the supported bilayer composition is 98% Egg-PC and 2% $\beta$-BODIPY FLC$_5$-HPC, and the composition of the upper bilayer patches is 98% Egg-PC and 2% $\beta$-BODIPY 581/591 $C_5$-HPC; for Figure 3 the supported bilayer composition is 96% DMPC, 2% DODAP, and 2% NBD-PG, and the composition of the upper bilayer patches is 99% DMPC, 0.5% Texas red DHPE, and 0.5% DODAP.
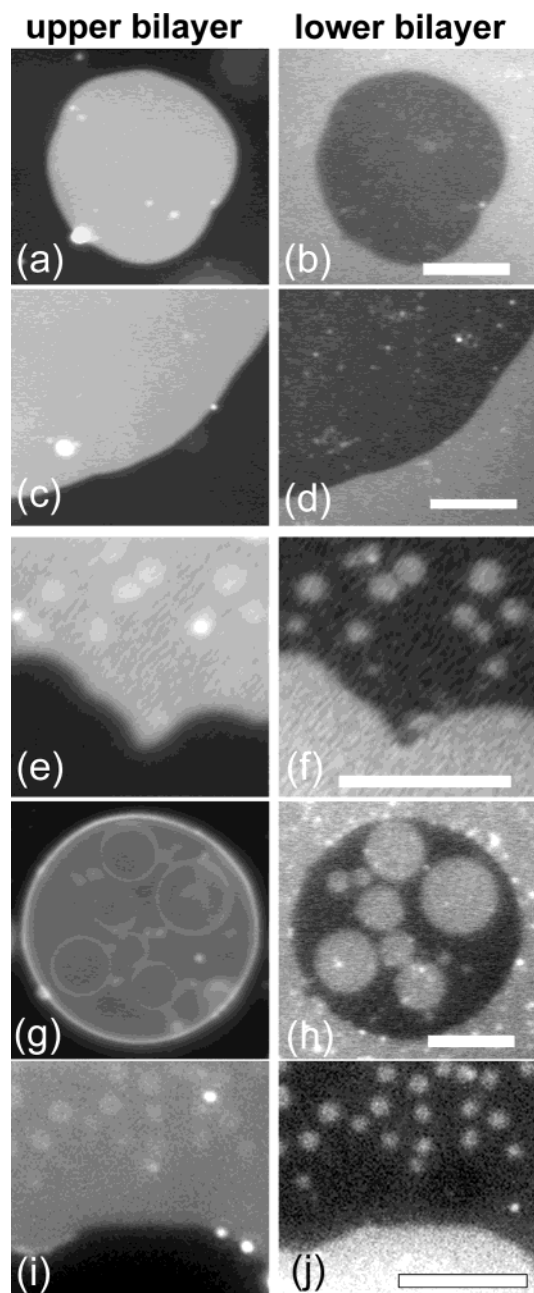
Preparation of SUVs, GUVs, and the resulting supported bilayers and upper bilayer patches has been described previously.[10,11,17] In brief, solutions of lipids in chloroform were mixed to the desired composition and the chloroform was then removed by evaporation. The resulting dried lipid films were hydrated with distilled, deionized water (2 mg/mL) at 4 °C for approximately 12 h. SUVs were formed either by sonication and ultracentrifugation (166 000*g*, 2.5 h, 4 °C) or by extrusion through 0.1 $\mu$m polycarbonate filters. GUVs were formed by hydration of the dried lipid films in 0.5 M sucrose solution (0.5 mg/mL), which was initially at 45 °C and was subsequently cooled to room temperature over approximately 12 h.

Supported bilayers were formed by rupture and fusion of SUVs onto glass coverslips or silicon oxide/silicon wafers, cleaned previously with piranha solution (3:1 concentrated sulfuric acid/30% hydrogen peroxide). The bilayers are always immersed in an aqueous environment. Typically, a few microliters of GUV suspension were dropped into the dish containing the supported bilayer. The GUVs sink because of the higher density of the sucrose solution; in close proximity to the supported bilayers, electrostatic, van der Waals, and other forces determine the bilayer–bilayer interaction. In some experiments, salt was added to the supported bilayer environment before the GUV deposition and was allowed to equilibrate. In experiments involving osmotic shock, droplets ($\approx$5 $\mu$l) of NaCl (1 M) or sucrose (0.5 M) were dropped onto the GUVs *following* their introduction to the supported bilayer environment.

For studies using FLIC, silicon wafers with a 100 nm thermal oxide layer were purchased from Silicon Quest (Santa Clara, California). As before, supported bilayers are formed on the oxide layer, which acts as a spacer between the lipid junction system and the reflective Si surface. Interference contrast in the fluorescence of the Texas red probes in the upper bilayer
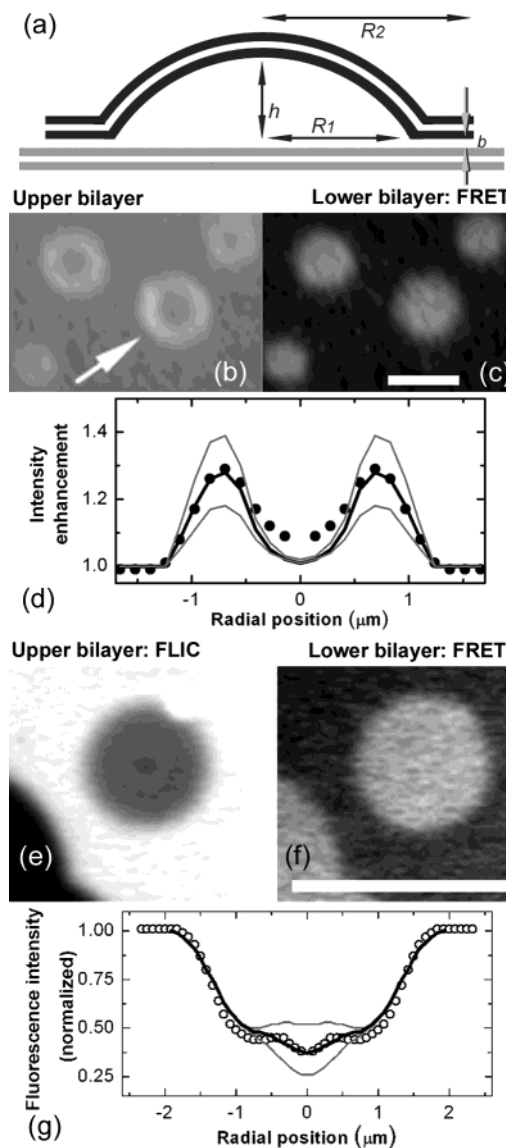


**Figure 1.** Blisters at bilayer–bilayer junctions. (a) Schematic diagram of the blister geometry (not to scale) showing the height (*h*) and radius ($R_1$) of a single blister as well as the extent of the upper bilayer patch ($R_2$, typically much greater than $R_1$) and the separation (*b*) between bilayers in regions of tight contact. (b) Fluorescence (Texas red DHPE) image of a section of an upper bilayer patch, shown to be continuous and unperforated. Blisters are evident as rings of enhanced fluorescence, as discussed in the text. (c) Fluorescence (NBD-PG) image of the lower supported bilayer in the same field of view as part b. The FRET footprint of the bilayer–bilayer contact zone is manifest as dark (quenched) fluorescence; the interbilayer spacing is *b* < 0.01 $\mu$m. Blisters are evident as bright, unquenched circles of fluorescence intensity. Scale bar = 2 $\mu$m. Bilayer compositions are given in Materials and Methods. (d) Intensity profile (circles) of the ring of enhanced intensity for the blister indicated by an arrow in part b. The lines are calculated intensity profiles, accounting for the blister geometry and microscope response function. The closest fit (thick line) indicates a blister of radius $R_1$ = 0.9 $\mu$m and height *h* = 0.5 $\mu$m; the thin lines are curves for *h* = 0.4 (below) and *h* = 0.6 $\mu$m (above), for comparison. (e) Fluorescence (Texas red DHPE) image, in interference contrast (FLIC) mode, of a blister in an upper bilayer patch; concentric rings of intensity demarcate height contours. (f) Fluorescence (NBD-PG) image of the lower supported bilayer in the same field of view as part e, again showing the FRET footprint of tight contact and a high-intensity circle at the blister location. Scale bar = 5 $\mu$m. (g) Intensity profile (circles) of the FLIC data from the blister in part e, together with the calculated profiles for blisters of radius $R_1$ = 1.25 $\mu$m and height *h* = 0.29 $\mu$m (black curve, best fit), *h* = 0.275 $\mu$m (gray, upper curve), and *h* = 0.305 $\mu$m (gray, lower curve).

Adhesion Patterns at Lipid Bilayer Junctions

*J. Phys. Chem. B, Vol. 108, No. 2, 2004* **651**

## upper bilayer    lower bilayer



**Figure 2.** In solutions of static osmotic strength, bilayer−bilayer contact is typically uniform (a−d). In contrast, osmotic shock delivered after the introduction of the GUVs leads to blisters in the bilayer−bilayer junction, as demonstrated by FRET (e−j); the junction shown in Figure 1 was also subjected to osmotic shock. The data of (e−j) were obtained by shock with concentrated (1 M) NaCl solution, as described in the text; similar blisters are formed by shock with concentrated sucrose solution. Scale bar = 10 $\mu$m. Blisters in bilayer−bilayer junctions can form in the absence of charged lipid components, illustrated in (i,j); the upper (left) and lower (right) bilayers are both composed of charge-neutral Egg-PC lipids and BODIPY fluorescent probes, as detailed in Materials and Methods.

patch is monitored, making use of an adjustable numerical aperture (NA 0.5−1.3) objective lens (Nikon, Tokyo, Japan).

Images were obtained at room temperature using a Nikon TE300 inverted fluorescence microscope (Nikon, Tokyo, Japan) with a Hamamatsu ORCA 2 (C4742-98) charge-coupled device camera (Hamamatsu, Tokyo, Japan) and Simple PCI acquisition software (Compix, Cranberry Township, Pennsylvania). Images were analyzed using Adobe Photoshop (Adobe Systems, San

Jose, California) and Metamorph (Universal Imaging, Down-ingtown, Pennsylvania). In the fluorescence images shown, a uniform background intensity has been subtracted to enhance the display contrast.

## 3. Results

**3.1. Blister Structure.** In Figure 1 we show images of blisters observed in bilayer−bilayer junctions, along with a schematic illustration of the blister structure (Figure 1a). On transparent substrates, the upper bilayer patch is shown to be continuous and unperforated (Figure 1b). The lower bilayer contains the NBD donor of the FRET pair (Figure 1c). The FRET footprint (dark) shows a large region of tight contact (less than 10 nm) between the membranes. Inside this footprint are zones of bilayer separation (bright circles) corresponding to blisters.

Especially for large blisters, under ideal optical focus evidence of the blister structure can be visible in the upper membrane fluorescence as a ring of high intensity at the blister periphery (Figure 1b). The ring results from the increased membrane area per projected viewing area along the line of sight at the blister edges. Treating the blister as a segment of a sphere of height $h$, radius $R_1$, and radius of curvature $R_c = (R_1^2 + h^2)/(2h)$, it is straightforward to calculate the enhanced blister fluorescence intensity as a function of the radial coordinate, $r$:

$$\text{Intensity} \sim (1.0 - r^2/R_1^2)^{-1/2} \qquad (1)$$

We convolve this intensity function with the microscope point spread function (PSF)[18]

$$\text{PSF} \sim (2J_1(v)/v)^2 \qquad (2)$$

where $J_1$ is the Bessel function of the first kind of order 1 and

$$v = \frac{2\pi}{\lambda_{em}} \frac{\text{NA}}{n_w} r \qquad (3)$$

Here, $\lambda_{em} = 620$ nm is the emission wavelength of the Texas red fluorophores, NA $= 0.9$ is the numerical aperture of the objective lens, and $n_w = 1.33$ is the index of refraction of water. Comparing the resulting calculated intensity profile with the observed profile allows extraction of the blister height, as illustrated in Figure 1d for the blister indicated by the arrow in Figure 1b, which has radius $R_1 = 0.9$ $\mu$m and height $h = 0.5$ $\mu$m.

Imaging with FLIC on reflective substrates provides an independent method of measuring blister topography. Fluorescence images from the lower supported bilayer again show FRET footprints (Figure 1f). The bright FRET domains correspond to nonuniform intensity in the FLIC image of the upper bilayer (Figure 1e); the interference patterns indicate a three-dimensional domed "blister" shape. Expressions for fluorescence intensity as a function of the distance between the fluorophore and the Si surface are derived following the analysis of Lambacher and Fromherz.[12] Accounting for polychromatic excitation and emission and a spread in illumination and detection angles given by the microscope optics, we calculate the intensity profile of a blister, again treated as a segment of a sphere, and convolve with the microscope point spread function (eqs 2 and 3, with NA = 0.5). We compare the resulting profile with the observed fluorescence intensity profile. This allows extraction of the blister height, as illustrated in Figure 1g for the blister of Figure 1e,f, which has radius $R_1 = 1.25 \pm 0.05$ $\mu$m and height $h = 0.29 \pm 0.01$ $\mu$m. (The stated uncertainties in $R_1$ and $h$ are estimates based on intensity profiles
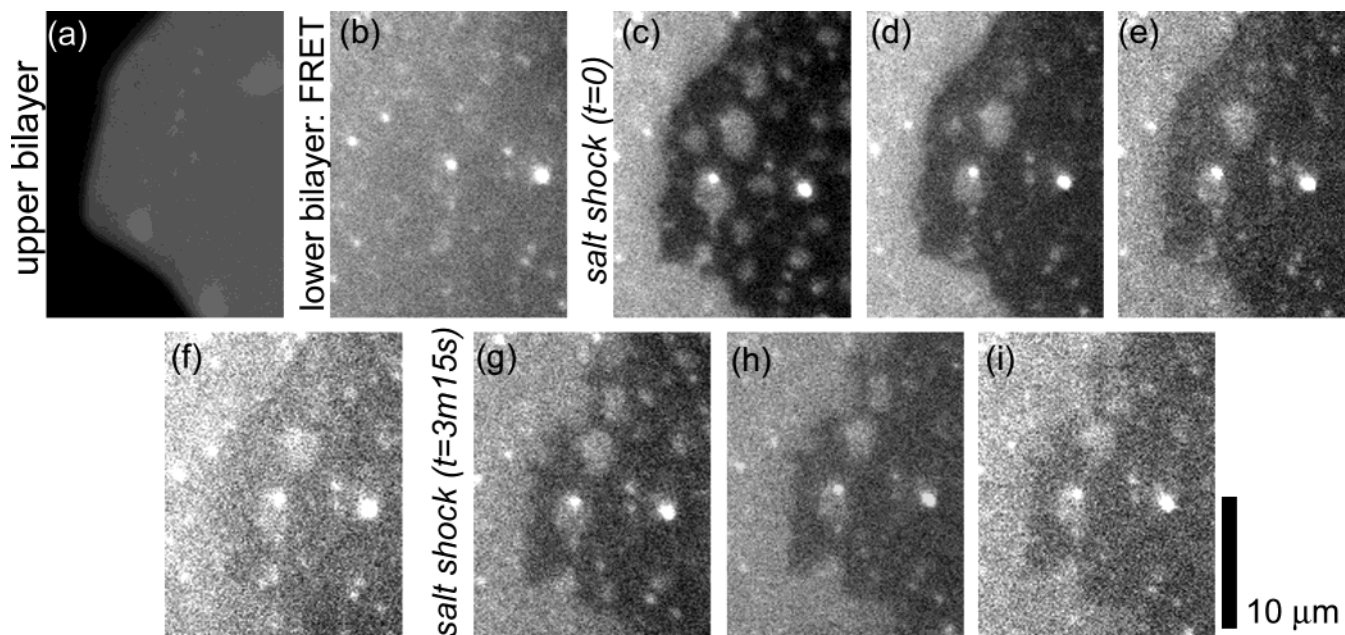
**Figure 3.** Repeated osmotic shock leads to repeated collapse of the upper bilayer. Part a shows an upper bilayer patch whose separation from the lower bilayer is outside the range of FRET so that there is no FRET footprint in the lower bilayer fluorescence shown in frame b. Salt shock leads to immediate tight contact between the bilayers, as indicated by the dark FRET signature in frame c. Blisters are evident in the junction as bright features. The upper bilayer slowly rises, returning towards its original separation, and the FRET footprint fades (shown in frames c−f; approximately 30 s between images). A second salt shock (preceding frame g) leads again to collapse of the upper bilayer patch shown in frame g, followed by another rise (shown in frames g−i; approximately 30 s between images).

such as those shown in Figure 1g. We do not consider the systematic uncertainty resulting from treatment of the blisters as perfect segments of spheres, which is the most likely cause of the slight discrepancy between the calculated and measured curves of Figure 1g.)

In regions of tight adhesion, the existence of the dark FRET footprint shows the interbilayer separation to be on the order of nanometers.[11] The blister heights, established independently by both conventional and fluorescence interference contrast microscopy, are much larger, on the order of hundreds of nanometers. This distinction is crucial to the blister stability, as we discuss later. FLIC also shows that the blisters are taut domes interspersed amid tightly adhered membranes.

**3.2. Osmotic Shock Produces Blisters.** The presence or absence of blisters in intermembrane junctions depends strongly on the conditions under which the lipid bilayers are brought together. In Figure 2 we show bilayer−bilayer junctions formed in solutions of static (a−d) and suddenly increased (e−j) osmotic strength. In the former setup, GUVs are introduced to the supported bilayer, which is immersed in a solution of static NaCl concentration (100 mM for Figure 2a−d). Rupture of the GUVs generally led to bilayer−bilayer junctions of uniform adhesion. In the latter setup, a few microliters of 1M NaCl were dropped into 3 mL of solution already containing GUVs, together with the supported bilayer and 0−100 mM NaCl. The shock generally led to rupture of the GUVs and bilayer−bilayer patches of nonuniform adhesion, that is, blisters (Figure 2e−j). The formation and structure of the blisters is the same for lipid compositions consisting mostly of saturated (DMPC) or of unsaturated (e.g., DOPC) lipids. Sucrose shock (droplets of 0.5 M sucrose) also led to blister formation. As will be discussed quantitatively later, solute shock creates an osmotic pressure which rapidly drives the ruptured upper bilayer patch towards the supported membrane.

The fall of the upper bilayer can be transient: the shock moves it away from its original separation from the lower

membrane, and it relaxes back. In Figure 3, for example, we show images from a bilayer−bilayer junction in which the steady state distance between the upper and lower bilayer is outside the FRET range. There is initially no FRET "footprint" in the lower bilayer fluorescence (Figure 3b). With a salt shock, the upper bilayer falls (Figure 3c) to a separation that is well within the Förster radius, and FRET maps the now tight contact zone, which is punctuated by blisters. Over the course of minutes, the upper bilayer patch rises back to its original spacing, and the FRET intensity diminishes (Figure 3c−f). Repeated salt shock of the same system causes repeated collapse of the upper bilayer, followed again by a slow rise (Figure 3g−i, as well as further repetitions that are not shown). While the blisters coarsen slightly with time (i.e., merge together), large ones remain fixed in position amid the repeated rising and falling of the upper bilayer patch. This fixedness is a consequence of the large height of the blisters relative to the small interbilayer separation in the tight adhesion zones. In upper bilayer patches formed from ruptured giant vesicles (e.g., Figure 2e,f,i,j and Figure 3), mild coarsening of the blisters with time is observed. In bilayer−bilayer junctions formed by intact giant vesicles that are simply deformed at the supported bilayer surface, there is much more coarsening (Figure 2g,h).

Blisters of the sort shown were first described by Nardi et al.,[14] who proposed reorganization of charged lipids as the driving force behind nonuniform adhesion. Our experiments reveal different mechanisms at play, which do not require charge reorganization. In experiments in which fluorescent probes are the only charged components of the upper bilayer patches, we find uniform fluorescence intensity, indicating uniform distribution of charge. Furthermore, we find blister formation in systems composed entirely of neutral or zwitterionic molecules: phosphatidylcholine lipids and "BODIPY" fluorescent probes (see Materials and Methods), as illustrated in Figure 2i,j.

Notably, alteration of the bilayer charge by Nardi and co-workers was obtained by adjusting the pH of the bilayer

Adhesion Patterns at Lipid Bilayer Junctions

*J. Phys. Chem. B, Vol. 108, No. 2, 2004* **653**
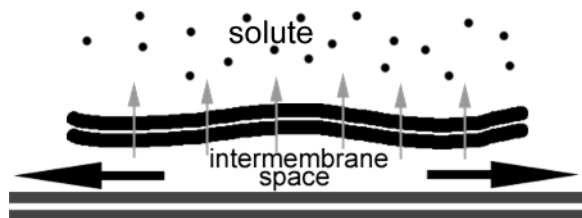


**Figure 4.** Osmotic shock leads to a high solute concentration above the upper bilayer (upper pair of lines, dark gray) and hence to an osmotic pressure pushing the bilayer patch towards the supported bilayer (lower pair of lines, light gray). This pressure can be relieved by permeation of water through the membrane (thin arrows) or lateral flow of fluid in the interbilayer space (thick arrows).

environment. Starting at low pH, the relevant lipid was uncharged; upon raising the pH it acquired a negative charge, and blisters were observed. A change in pH, however, changes the ionic strength of the solution. As discussed previously, osmotic shock alone is sufficient to induce blister formation.

## 4. Discussion

The central questions concerning the intermembrane junction blisters are these: what creates them and how are they stabilized?

**4.1. Blister Formation.** Osmotic shock induces strong and rapid attraction between the two bilayers. The dense droplet of NaCl or sucrose solution creates a high solute concentration immediately above the upper bilayer, causing an osmotic pressure that pushes it downward (Figure 4). It is therefore energetically preferable to reduce the amount of water in the interbilayer space. This transport of water can be achieved either by permeation of water through the upper membrane or by lateral flow of water beyond the upper bilayer patch boundary. (Permeation of solute through the bilayer is several orders of magnitude slower than permeation of water.) The osmotic pressure, meanwhile, is reduced by the diffusion of ions around the bilayer patch into the interbilayer space and also into the surrounding aqueous environment. The time scale needed for the diffusion of ions to equalize the osmotic strength on both sides of the upper bilayer patch is given roughly by

$$t_D \approx R_2^2/D_i \tag{4}$$

where $R_2$ is the radius of the upper bilayer patch and $D_i$ is the diffusion constant for the ions. The values $R_2 \approx 5$ $\mu$m and $D_i \sim 10^3$ $\mu$m$^2$/s give $t_D \approx 0.03$ s.

The time scale for permeation of water is set by the permeability of the lipid bilayer to water ($\lambda \approx 50$ $\mu$m/s)[19] and the osmolarity difference across the bilayer ($\Delta c$):

$$\frac{dV}{dt} = -A\lambda\frac{\Delta c}{c} \tag{5}$$

where $V$ is the volume of water in the interbilayer space, $A$ is the area of the upper membrane patch, and $c$ is the concentration of pure water ($c = 55.4$ M). Writing $V = Ay$, where $y$ is the interbilayer separation, and neglecting diffusion, the time scale $t_{p1}$ for permeation for an initial separation $y_0$ is approximately

$$t_{p1} \approx \frac{y_0}{\lambda(\Delta c/c)} \tag{6}$$

from which $t_{p1}/[s] \approx y_0/[\mu m]$ for an osmolarity difference $\Delta c$



**Figure 5.** Once a blister is formed, it can relax via permeation of water through the membrane (thin arrows) or expulsion of water through the tight interbilayer space, driven by the bilayer bending energy (thick arrows). As discussed in the text, each relaxation mechanism is effective only for very small blisters; hence, large blisters cannot relax and are stable on experimental time scales.

$\approx 1$ M. Note that diffusion of ions lowers $\Delta c$ so that the preceding expression for $t_{p1}$ is a rough lower bound. A characteristic $y_0 \approx 10$ nm gives $t_{p1} > 0.01$ s.

The time scale for bilayer motion via lateral expulsion of fluid from the interbilayer space is given approximately by

$$t_m \approx \frac{9\mu R_2^2}{\Delta c R_g T y_0^2} \tag{7}$$

(derived in the Appendix), where $\mu = 10^{-3}$ Pa·s is the viscosity of water, $R_g$ is the gas constant, $T$ is the temperature, and $y_0 \approx 10$ nm is again the initial separation distance of the membranes. The osmotic pressure $P_{osm} = \Delta c R_g T \approx 10^6$ Pa for $\Delta c \approx 1$ M and $T = 290$ K. The numerical values give $t_m \approx 10^{-3}$ s. (The value given for $\mu$ is the viscosity of bulk water. Near surfaces, especially in the narrow interbilayer space, the effective viscosity may be larger.)

Comparing the time scales for bilayer motion, $t_{p1}$ and especially $t_m$, with the diffusional time scale $t_D$, we see that well before the osmolarity gradient across the upper bilayer is equalized the upper bilayer patch can rapidly collapse towards the lower supported bilayer. The collapse is facilitated primarily by lateral fluid flow, rather than permeation.

Considering contact between flexible membranes separated by a thin fluid layer, Coakley, Ramos-de-Souza, and co-workers[20,21] have shown that spatial instabilities in the intermembrane spacing can generally develop as a consequence of strong adhesion or attraction, in our case, the rapid contact induced by osmotic shock. While the forces between membranes (van der Waals, electrostatic, hydration, etc.) define a uniform equilibrium separation, this equilibrium is unstable to large wavelength perturbations, which can grow into the nonuniform spacings observed here as blisters. Inhomogeneities in membrane–membrane separation are part of a more general class of well-studied instabilities in thin fluid films that result from competing attractive and repulsive forces.[22,23]

**4.2. Blister Stability.** Blisters are nonequilibrium structures, and their presence costs the upper bilayer membrane bending energy. Why, then, does the membrane not relax into an uncurved shape, flattening the blisters to achieve a uniform adhesion to the lower membrane? We might imagine two types of mechanisms (both already introduced in the context of motion of the *entire* bilayer patch) by which such a relaxation could be accomplished: permeation of water through the membrane and lateral drainage of fluid through the interbilayer space (Figure 5). We will examine the dynamics of both mechanisms, considering a blister of radius $R_1$ and height $h$, modeled as a segment of a sphere with radius of curvature $R_c = (R_1^2 + h^2)/2h$ (Figure 1a). It is straightforward to derive expressions for

the blister volume ($V_b$) and surface area ($A_b$):

$$A_b = 2\pi h R_c = \pi R_1^2\left(1 + \frac{h^2}{R_1^2}\right) \tag{8}$$

$$V_b = \pi h^2 R_c\left(1 - \frac{h}{3R_c}\right) = \frac{\pi}{2}hR_1^2\left(1 + \frac{h^2}{3R_1^2}\right) \tag{9}$$

The height of the blister is small compared to its radius ($h \ll R_1$) and becomes smaller still as the blister volume shrinks. Therefore,

$$V_b/A_b \approx h/2 \tag{10}$$

The blister empties by reducing its height, while keeping $R_1$ fixed. As seen in Figures 1 and 2, pinning sites generally fix the boundaries of the upper bilayer patches.

Permeation can be driven by the osmotic pressure imposed by the salt shocks that drive blister formation or by the mechanical pressure of the curved blister geometry. The osmotic pressure $P_{osm} \approx 10^6$ Pa, as calculated earlier. The mechanical pressure, derived in the Appendix, is roughly

$$P_m \approx \frac{k_c}{hR_c^2} \approx 10^{-2}\text{ Pa} \tag{11}$$

using $k_c \approx 10^{-19}$ J for the bending modulus of the lipid bilayer and characteristic values $h \approx 100$ nm and $R_c \approx 10$ $\mu$m. The mechanical pressure is far less than the osmotic pressure and so can be neglected when considering permeation. The time scale for the blister to empty by permeation is calculated via eqs 5 and 10, from which

$$\frac{dh}{dt} = -4\lambda\frac{\Delta c}{c} \tag{12}$$

Again neglecting diffusion of ions and treating $\Delta c$ as fixed in time, we obtain a lower bound on the time scale for a blister of height $h_0$ to empty by permeation:

$$t_{p2} \approx \frac{h_0}{4\lambda\frac{\Delta c}{c}} \tag{13}$$

which gives $t_{p2}/[\text{s}] \approx (h_0/4)/[\mu\text{m}]$. A blister of height $h_0 = 400$ nm would need 0.1 s to empty by permeation, if the salt concentration immediately above the bilayer patch remained fixed at 1 M. Given the rapid diffusion time scale ($t_D \approx 0.03$ s), the permeation time is undoubtedly considerably longer than the value given by eq 13, and only the shallowest blisters can expel their contents by membrane permeation.

The second mechanism of blister relaxation is drainage of fluid through the intermembrane space, the force being provided by the membrane bending energy of the blister. Notably, this mechanism has not been realized in previous models, which employed periodic boundary conditions that miss drainage and other such boundary-dependent effects. The time scale for blister drainage, $t_b$, is determined by the bilayer bending modulus, the blister geometry, and the viscosity of the expelled water. It is derived in the Appendix to be given approximately by

$$t_b \approx \frac{3}{2}\frac{\mu}{k_c b^3}R_1^6 \ln\left(\frac{R_2}{R_1}\right) \tag{14}$$
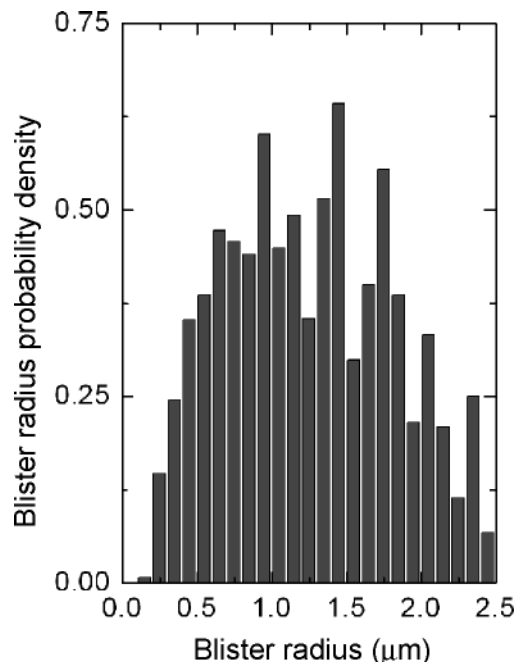


**Figure 6.** The probability distribution of blister sizes, obtained from images of about 1200 blisters. The data show a drop in blister occurrence for radii below around 0.5 $\mu$u, consistent with our calculations that small blisters can drain rapidly and disappear, while large blisters cannot. The drop in the size distribution occurs above the resolution limit of the observations ($R_1 \approx 0.25$ $\mu$m). The probability distribution also drops at large radii because of the finite size of the upper bilayer patches.

where $\mu$ is the fluid viscosity, $k_c$ is the membrane bending modulus, $b$ is the interbilayer separation in the tightly adhered junction (away from the blister), $R_1$ is the blister radius, and $R_2$ is the radius of the entire upper bilayer patch. The most striking feature of the drainage time scale is the sharp dependence on blister radius, which is a consequence of the fact that the volume to be drained increases with $R_1$ and the pressure applied by the curved membrane decreases with $R_1$. Ignoring the weak logarithmic factor in eq 14 and using $b \approx 10$ nm,

$$t_b \sim 10^4(R_1/[\mu\text{m}])^6 \tag{15}$$

Blisters smaller than roughly $R_1^* \approx 400$ nm can drain within the experimental window (on the order of 1 min), while those larger cannot. We would expect, therefore, to observe many blisters of radii $R_1 > R_1^*$, while smaller blisters would have already drained and disappeared. This idea is consistent with Figure 6, where the probability distribution $P(R_1)$ is determined from measurements of the radii ($R_1$) of 1200 blisters. The distribution falls off for $R_1$ less than roughly 0.5 $\mu$m. (We note that some of this decline must be due to coarsening of small blisters as well.) $P(R_1)$ also drops for large $R_1$, presumably due to the finite size of the upper bilayer patches and also the low likelihood of creating arbitrarily large blisters.

## 5. Conclusions

Combined application of FRET and FLIC imaging allows investigation of multiple length scales in concert at intermembrane contacts. Using these techniques, we have probed nonequilibrium "blister" structures, hundreds of nanometers in height, that can form at the otherwise few nanometer-spaced junctions between simple lipid bilayers. Blister formation is triggered by strong, rapid adhesion between the membranes and

Adhesion Patterns at Lipid Bilayer Junctions

*J. Phys. Chem. B, Vol. 108, No. 2, 2004* **655**

need not have any correlation with the phase separation or motion of charged lipids in the bilayer. This mechanism of shock-induced nonuniform adhesion and the charge reorganization model of Nardi et al. may provide alternative and independent pathways towards nonuniform adhesion in soft membrane systems. Our observations and model suggest that the stability of these blisters is enforced by fluid dynamics: the time scales for blister drainage determine relaxation kinetics and are exceptionally long for large blisters.

The ramifications of these studies are twofold. First, since nonuniform adhesion and its stabilization by fluid impedance are independent of the details of membrane composition, they may be generally relevant to systems involving membrane—membrane adhesion, even in the presence of other, more complex interactions. In neural synapses,[4] for example, we see an inspiring interplay of adhesion, structure formation, and fluid flow (neurotransmitter release in the synaptic cleft), which may be amenable to analyses such as these. Second, blisters in reconstituted lipid bilayer junctions, as regions of large and well-defined spacing from other surfaces, provide unique and varied environments in which the behavior of phase-separated lipid domains (rafts), membrane-associated proteins, and other objects of biophysical interest may be investigated.

## 6. Appendix: Fluid Flow in the Interbilayer Space

We consider laminar flow of water in the interbilayer space, first in the context of the flow driven by the bending energy of a draining blister (deriving eq 14) and then in the context of osmotic pressure pushing the entire bilayer patch towards the supported membrane (deriving eq 7).

**6.1. Drainage of Fluid.** We first relate fluid flow to pressure in the narrow interbilayer space. Considering for simplicity a radially symmetric zone of tight contact (either a flat upper membrane patch or the region of tight contact surrounding a blister), the radial flow of water is related to the fluid pressure ($p = p(r)$, where $r$ is the radial coordinate) at low Reynolds number by the creeping flow equation:

$$\vec{\nabla}p = \mu\nabla^2\vec{v} \tag{16}$$

where $\vec{v}$ is the flow velocity and $\mu$ is the viscosity. Continuity, $\nabla\cdot\vec{v} = 0$, requires that

$$\nabla\cdot\vec{v} = \frac{1}{r}\frac{\partial}{\partial r}(rv_r) = 0 \tag{17}$$

which forces the velocity to follow

$$v(r) = c_0/r \tag{18}$$

where $c_0$ is some constant. Then eqs 16 and 18 combine to give

$$\frac{\partial p}{\partial r} = \mu\frac{\partial^2 v}{\partial y^2} \tag{19}$$

where $y$ is the coordinate perpendicular to the bilayer plane,

with the terms involving $c_0$ canceling out. Since the pressure has no $y$-dependence, the general solution to this expression is

$$v(r, y) = \frac{1}{2\mu}\frac{\partial p}{\partial r}y^2 + c_1 y + c_2 \tag{20}$$

with $c_1$ and $c_2$ as constants. Applying no-slip boundary conditions ($v(y = 0) = v(y = b) = 0$ at all $r$), we see that $c_2 = 0$ and $c_1 = (-{}^1/_2\mu)(\partial p/\partial r)b$, with $b$ being the separation between the membranes in tight contact. Thus,

$$v_r(r, y) = \frac{1}{2\mu}\frac{\partial p}{\partial r}(y^2 - by) \tag{21}$$

The average velocity ($u(r)$) at radial coordinate $r$ is

$$u(r) = \frac{1}{b}\int_0^b v_r(r, y)\,\mathrm{d}y = -\left(\frac{b^2}{12\mu}\frac{\partial p}{\partial r}\right) \tag{22}$$

This relates the mean radial fluid velocity to the radial pressure gradient. The mean velocity $u(r)$, like $v(r, y)$, must go as $1/r$, so

$$u(r) = c/r \tag{23}$$

where $c$ is a constant. Therefore, eq 22 then becomes

$$\frac{\partial p}{\partial r} = -\left(\frac{12\mu c}{b^2}\right)\frac{1}{r} \tag{24}$$

which we integrate from $r = R_1$, at which point $p(R_1) = p_0$ (defining $p_0$ as the interior pressure), to arbitrary $r$ to get

$$p(r) = p_0 - \left(\frac{12\mu c}{b^2}\right)\ln(r/R_1) \tag{25}$$

In the blister geometry, $R_1$ is the radius of the blister (see Figure 1a) and $R_2$ is the radius of the bilayer patch. Writing $p(R_2) = 0$, we solve for $c$:

$$c = \frac{b^2 p_0}{12\mu}[\ln(R_2/R_1)]^{-1} \tag{26}$$

We have now related the flow velocity between the disks to the pressure driving the flow via eqs 23−26.

**6.2. Blister Bending Energy and Fluid Flow.** We next examine the source of the pressure. First we determine the drainage time for a blister, driven by the bending energy of the curved blister. The geometry is given in Figure 1a, and expressions for the volume and surface area are given in eqs 8 and 9.

The membrane bending energy $E_b$ is given by

$$\frac{E_b}{A} = \frac{k_c}{2}\left(\frac{1}{R_\alpha} + \frac{1}{R_\beta}\right)^2 \tag{27}$$

where $A$ is the surface area of the deformed membrane, $k_c$ is the bending modulus, and $R_\alpha$ and $R_\beta$ are the radii of curvature along perpendicular directions. For our blisters, $R_\alpha = R_\beta \equiv R_c$. Therefore, from eq 8,

$$E_b = \pi k_c(h/R_c) \tag{28}$$

The inward force applied by the blister is

$$F \approx \mathrm{d}E_b/\mathrm{d}h = \pi k_c/R_c \tag{29}$$

treating $R_c$ as constant. The pressure, therefore, in the fluid below

**656** *J. Phys. Chem. B, Vol. 108, No. 2, 2004*

Parthasarathy et al.

the blister surface is

$$p_0 = F/A = \frac{k_c}{2hR_c^2} \tag{30}$$

Now we have the pressure in terms of the blister geometry and the fluid flow in terms of the pressure. Next, we will combine these relations. As noted earlier, we treat the blister radius $R_1$ as fixed, while its height ($h$) drops as it drains.

Considering fluid in an annulus of the disk (of radius $r$ and width $dr$), in time $dt = dr/u(r)$ we move a volume $dV_{disk} = b2\pi r\, dr$; therefore, the blister volume ($V_b$) is diminished by this amount, and

$$dV_b = -2\pi bru(r)\, dt \tag{31}$$

$$dt = -dV_b\, \frac{12\mu}{\pi b^3} \ln\!\left(\frac{R_2}{R_1}\right)\frac{hR_c^2}{k_c} \tag{32}$$

From eq 9,

$$\frac{dV_b}{dh} = \frac{\pi}{2}R_1^2\!\left(1 + \frac{h^2}{R_1^2}\right). \tag{33}$$

Thus, also noting that $R_c = (R_1^2 + h^2)/2h$,

$$dt = -\frac{3}{2}\frac{\mu}{k_c b^3} \ln\!\left(\frac{R_2}{R_1}\right)R_1^6 \frac{dh}{h}\!\left(1 + \frac{h^2}{R_1^2}\right)^3 \tag{34}$$

The height of the blister is small compared to its radius ($h \ll R_1$) and becomes smaller still as the blister drains. Therefore, we can neglect $h^2/R_1^2$. Also, defining

$$t_b = \frac{3}{2}\frac{\mu}{k_c b^3} \ln\!\left(\frac{R_2}{R_1}\right)R_1^6 \tag{35}$$

which has dimensions of time, we obtain

$$dt \approx -t_b(dh/h) \tag{36}$$

If the blister starts at height $h = h_0$ at time $t = 0$, it decays exponentially with time constant $t_b$

$$h(t) = h_0 \exp(-t/t_b) \tag{37}$$

Thus, eqs 35 and 37 describe the blister drainage.

**6.3. Collapse of the Upper Bilayer.** Our fluid flow expressions can also be used to estimate the time scale for collapse of the upper bilayer following osmotic shock. As calculated earlier, the osmotic pressure resulting from a $\Delta c \approx 1$ M salt droplet above the membrane patch is $P_{osm} = \Delta c R_g T \approx 10^6$ Pa, which forces the bilayer patch towards the lower membrane. The dominant drag on this motion comes from the fluid flow in the interbilayer space. We approximate the fluid flow as radial, to obtain a rough estimate of the bilayer collapse time scale. As in eq 23, the flow velocity $u(r) \approx c/r$, where the constant

$$c = \frac{P_{osm}y^2}{12\mu} \tag{38}$$

Note that we write the bilayer−bilayer separation, which is not constant as the bilayer falls, as $y$. Flow reduces the volume in the interbilayer space:

$$dV = -2\pi yru(r)\, dt \tag{39}$$

As $V = \pi R^2 y$, where $R$ is the radius of the bilayer patch ($R_2$ above),

$$dy = -\frac{P_{osm}y^3}{6R^2\mu}\, dt \tag{40}$$

Integrating from an initial separation $y_0$ to $y_0/2$, we obtain a characteristic time scale for collapse

$$t_m \approx \frac{9\mu R^2}{P_{osm}y_0^2} \tag{41}$$

$$= \frac{9\mu R^2}{\Delta c R_g T y_0^2} \tag{42}$$

which is eq 7. Numerically, $R \approx 5$ μm, $\Delta c \approx 1$ M, $\mu = 10^{-3}$ Pa·s, and $y_0 \approx 10$ nm, giving $t_m \approx 10^{-3}$ s.

**References and Notes**

(1) Sackmann, E.; Bruinsma, R. F. Cell Adhesion as Wetting Transition? *ChemPhysChem.* **2002**, *3*, 262−269.

(2) Singer, S. J. Intercellular Communication and Cell−Cell Adhesion. *Science* **1992**, *255*, 1671−1677.

(3) Grakoui, A.; Bromley, S. K.; Sumen, C.; Davis, M. M.; Shaw, A. S.; Allen, P. M.; Dustin, M. L. The Immunological Synapse: A Molecular Machine Controlling T-Cell Activation. *Science* **1999**, *285*, 221−227.

(4) Dustin, M. L.; Colman, D. R. Neural and Immunological Synaptic Relations. *Science* **2002**, *298*, 785−789.

(5) Qi, S. Y.; Groves, J. T.; Chakraborty, A. K. Synaptic Pattern Formation during Cellular Recognition. *Proc. Natl. Acad. Sci. U.S.A.* **2001** *98*, 6548−6553.

(6) Lee, S. E.; Hori, Y.; Groves, J. T.; Dustin, M. L.; Chakraborty, A. K. Correlation of a Dynamic Model for Immunological Synapse Formation with Effector Functions: Two Pathways to Synapse Formation. *Trends Immunol.* **2002**, *23*, 492−499.

(7) Weikl, T. R.; Groves, J. T.; Lipowsky, R. Pattern Formation during Adhesion of Multicomponent Membranes. *Europhys. Lett.* **2002**, *59*, 916−922.

(8) Sackmann, E. Supported Membranes: Scientific and Practical Applications. *Science* **1996**, *271*, 43−48.

(9) Niles, W. D.; Silvius, J. R.; Cohen, F. S. Resonance Energy Transfer Imaging of Phospholipid Vesicle Interaction with a Planar Phospholipid Membrane: Undulations and Attachment Sites in the Region of Calcium-Mediated Membrane−Membrane Adhesion. *J. Gen. Physiol.* **1996**, *107*, 329−351.

(10) Wong, A. P.; Groves, J. T. Topographical Imaging of an Intermembrane Junction by Combined Fluorescence Interference and Energy Transfer Microscopies. *J. Am. Chem. Soc.* **2001** *123*, 12414−12415.

(11) Wong, A. P.; Groves, J. T. Molecular Topography Imaging by Intermembrane Fluorescence Resonance Energy Transfer. *Proc. Natl. Acad. Sci. U.S.A.* **2002**, *99*, 14147−14152.

(12) (a) Lambacher, A.; Fromherz, P. Fluorescence Interference-Contrast Microscopy on Oxidized Silicon Using a Monomolecular Dye Layer. *Appl. Phys. A* **1996**, *63*, 207−216. (b) Lambacher, A.; Fromherz, P. Luminescence of Dye Molecules on Oxidized Silicon and Fluorescence Interference Contrast Microscopy of Biomembranes. *J. Opt. Soc. Am. B* **2002**, *19*, 1435−1453. Both papers provide expressions for fluorescence intensity as a function of distance of the fluorophore from the reflective substrate, considering the optics of interference at an imperfectly reflective surface, orientations of fluorophore excitation and emission dipoles, and finite spreads in the directions and wavelengths of excitation and emission light. Ref b also considers nonradiative energy transfer from the fluorophore to the Si surface, which is negligible for the conditions of this experiment. Although we use the full FLIC analysis in this paper, we note that the simplest expression for FLIC intensity for a fluorophore at height $z$ above the oxide layer is given by

$$\text{Intensity} \sim \sin^2\!\left(\frac{2\pi}{\lambda_{ex}}(n_o z_o + n_w z_w)\right)\sin^2\!\left(\frac{2\pi}{\lambda_{em}}(n_o z_o + n_w z_w)\right) \tag{43}$$

where $\lambda_{ex}$ and $\lambda_{em}$ are the excitation and emission wavelengths for the fluorophores, $z_o$ is the oxide thickness, and $n_o$ and $n_w$ are the indices of refraction for $SiO_2$ and water, respectively. This approximation treats the excitation and emission light as monochromatic and normal to a perfectly reflecting surface. For our setup ($z_o = 100$ nm, $n_o = 1.46$, $n_w = 1.33$, mean

Adhesion Patterns at Lipid Bilayer Junctions

*J. Phys. Chem. B, Vol. 108, No. 2, 2004* **657**

wavelengths $\lambda_{ex}$ = 570 nm, $\lambda_{em}$ = 620 nm), we find that this simple expression and the full analysis give similar results, with the largest discrepancy arising because of the imperfect reflection of light at the Si surface.

(13) Rädler, J.; Sackmann, E. Imaging Optical Thicknesses and Separation Distances of Phospholipid Vesicles at Solid Surfaces. *J. Phys. II* **1993**, *3*, 727−748.

(14) Nardi, J.; Bruinsma, R.; Sackmann, E. Adhesion-Induced Reorganization of Charged Fluid Membranes. *Phys. Rev. E* **1998** *58*, 6340−6354.

(15) Bayerl, T. M.; Bloom, M. Physical Properties of Single Phospholipid Bilayers Adsorbed to Micro Glass Beads. *Biophys. J.* **1990**, *58*, 357−362.

(16) Koenig, B. W.; Krueger, S.; Orts, W. J.; Majkrzak, C. F.; Berk, N. F.; Silverton, J. V.; Gawrisch, K. Neutron Reflectivity and Atomic Force Microscopy Studies of a Lipid Bilayer in Water Adsorbed to the Surface of a Silicon Single Crystal. *Langmuir* **1996**, *12*, 1346−1350.

(17) Akashi, K.; Hidetake, M.; Hiroyasu, I.; Kinosita, K. Preparation of Giant Liposomes in Physiological Conditions and their Characterization under an Optical Microscope. *Biophys. J.* **1996**, *71*, 3242−3250.

(18) Gu, M. *Advanced Optical Imaging Theory*; Springer: Heidelberg, Germany, 2000.

(19) Olbrich, K.; Rawicz, W.; Needham, D.; Evans, E. Water Permeability and Mechanical Strength of Polyunsaturated Lipid Bilayers. *Biophys. J.* **2000**, *79*, 321−327.

(20) Coakley, W. T.; Gallez, D.; Ramos de Souza, E.; Gauci, H. Ionic Strength Dependence of Localized Contact Formation between Membranes: Nonlinear Theory and Experiment. *Biophys. J.* **1999**, *77*, 817−828.

(21) Ramos-de-Souza, E.; Anteneodo, C.; Gallez, D.; Bisch, P. M. Long-Scale Evolution of Thin Liquid Films Bounded by a Viscous Phase with Diffusing Charged Surfactants. *J. Colloid Interface Sci.* **2001**, *244* 303−312.

(22) Oron, A.; Davis, S. H.; Bankoff, S. G. Long-Scale Evolution of Thin Liquid Films. *Rev. Mod. Phys.* **1997**, *69*, 931−980.

(23) Sharma, A.; Khanna, R. Pattern Formation in Unstable Thin Liquid Films. *Phys. Rev. Lett.* **1998**, *81*, 3463−3466.